J. Plasma Physics (2013), vol. 79, part 5, pp. 699–713. © Cambridge University Press 2013
doi:10.1017/S0022377813000317

Modeling of electric arcs: A study of the non-convective case with strong coupling

D. WRIGHT[1], P. DELMONT[2] and M. TORRILHON[2]

[1]Seminar for Applied Mathematics, ETH Zürich, Rämistr. 101, 8092 Zurich, Switzerland
[2]MathCCES, RWTH Aachen University, Schinkelstr. 2, 52062 Aachen, Germany
(delmont@mathcces.rwth-aachen.de)

(Received 17 January 2013; revised 15 February 2013; accepted 18 February 2013; first published online 21 March 2013)

Abstract. In this paper, we investigate a mathematical model for electric arcs. The model is based on the equations of magnetohydrodynamics, where the flow and heat transfer in a plasma is coupled to electrodynamics. Our approach neglects convection and yields a reaction–diffusion model that includes only the core phenomena of electric arcs: Ohmic heating and nonlinear electric conductivity. The equations exhibit interesting mathematical properties like non-unique steady states and instabilities that can be linked to electric arc properties. Additionally, a 3D axisymmetric simulation of the creation and extinction of an electric arc is presented based on a strongly coupled numerical algorithm for the non-convective model. The approach is especially suited for high-current arcs where strong coupling becomes necessary.

1. Introduction

An electric arc is a discharge phenomenon in which current is conducted through a hot-ionized gas between an anode and a cathode. Typically, the temperature of the cathode is high enough so that electrons are emitted with almost no additional external force. The ionized gas forms a plasma which interacts with electric and magnetic fields of the current. Electric arcs occur increasingly in various industrial applications from melting, drilling, lighting to circuit breakers and electric thrusters. Hence, mathematical plasma modeling and plasma simulations are becoming increasingly important (for a review of the matter, see Gleizes et al. 2005). Electric arcs have been studied from the fundamental and experimental physics perspectives in the middle of the 20th century with classical publications (e.g. Cassie 1939; Mayr 1943; Maecker 1951; Mayr 1955; Finkelnburger and Maecker 1956; Rieder 1967). More modern, full arc simulations can be found for example in Kosse et al. (2007) and Zheng et al. (2004).

Some of the strongest electric arcs in technical processes are found in high performance circuit breakers with currents up to 200 kA and energies up to 1500 MW (see Van Der Sluis 2001; Garzon 2002; Zehnder et al. 2002). The largest of these breakers are installed in power plants to switch fault currents in emergencies in order to prevent damage to the interior of the plant resulting from an overload. Since it is impossible to prevent the creation of the electric arc when separating the contacts, a circuit breaker is designed to extinguish the arc as fast as possible once it is created. The two dissertations Huguenot (2008) and Kumar (2009) aim at the detailed and full-scale simulation of high-current electric arcs in high performance circuit breakers. In the theses, some proof of concepts could be given, but it also became clear that the simulation of this multi-physics process requires additional basic research in mathematical modeling and numerical analysis.

This paper starts with the equations of single-fluid real plasma magnetohydrodynamics (MHD) to study the fundamental mathematical mechanisms of electric arcs. As first step, a non-convective model is derived from the MHD equations under the assumption that the motion of the plasma is negligible. A future paper will extend the present results to plasma convection. The non-convective model is based on nonlinear electric conductivity and Ohmic heating as the fundamental mechanisms in the electric arc. The study of axisymmetric arcs then allows us to study the stability of electric arc. In that way, the creation and extinction of the arc can be viewed as an interplay of stable and unstable solutions to a system of reaction–diffusion equations, see also Torrilhon (2007). A 3D axisymmetric simulation demonstrates the usefulness of the model in more realistic geometries. Special attention is paid to the possibility to switch from voltage-driven to current-driven according to requirements from the external electric network. This requires to change the boundary conditions of the magnetic field accordingly.

Typically, in arc simulations, the equations of electrodynamics are coupled weakly to the flow and heat transfer, that is, the systems are often solved in a split way and Lorentz force and Ohmic heating transferred as external productions per time-step. This paper uses a strong coupling in which heat transfer and

electrodynamics are solved in a fully coupled way using a single implicit time integration. In this approach, the splitting is not introduced between heat conducting flow and electrodynamics, but between Ohmic heating and current diffusion on the one hand and non-dissipative effects like the flow on the other hand. This follows the argument that the arc is driven by Ohmic heating and nonlinear current diffusion, while the flow can be considered a reaction. As a result, the numerical method becomes more stable and robust especially for very high current situations.

As mentioned above, the presented model needs to be coupled to the plasma flow. However, the non-convective model can help to understand full-scale arc simulations better and may have relevant applications. For instance, initialization with a burning arc proved most difficult in Huguenot (2008) and Kumar (2009). A physical approach to create the electric arc as presented in this paper may be beneficial in these simulations. The model presented in this paper can also be coupled to an external electric network (see Delmont and Torrilhon 2012b) and used to advance black-box Cassie–Mayr models, as in Tseng et al. (1997) and Maximov et al. (2009). First convective simulations have also been published (see Delmont and Torrilhon 2012a).

The rest of the paper is organized as follows. We simplify the equations of dissipative and resistive MHD for the case of a non-convective arc and discuss the modeling and scaling in the next section. Then, Sec. 3 specializes the equations for an infinite axisymmetric arc column and we study steady (Sec. 4) and unsteady (Sec. 5) solutions and their stability. Section 6 describes 3D axisymmetric simulations. The paper ends with a conclusion.

2. Magnetohydrodynamics

In MHD, plasma is described on the basis of a single gas that models the electrical, chemical and thermodynamical behavior of the mixture of ions and electrons as a whole (see Goedbloed and Poedts 2004). MHD considers the fields of density ρ, velocity $\mathbf{v}$, temperature T, and magnetic field $\mathbf{B}$.

2.1. Equations

The equations of MHD are given by the conservation laws of mass, momentum and energy for the plasma and Maxwell's equation in eddy current approximation, that is, neglecting the displacement current. They read

$$\begin{aligned}
&\partial_t \rho + \operatorname{div} \rho\mathbf{v} = \mathbf{0},\\
&\partial_t \rho\mathbf{v} + \operatorname{div}(\rho\mathbf{v}\mathbf{v} + p\,\mathbf{I} + \Pi) = \mathbf{j}\times\mathbf{B},\\
&\partial_t \rho\left(\varepsilon + \tfrac{1}{2}\mathbf{v}^2\right) + \operatorname{div}\left(\rho\mathbf{v}\left(\varepsilon + \tfrac{1}{2}\mathbf{v}^2 + p\right) + \Pi\cdot\mathbf{v} + \mathbf{q}\right)\\
&\quad = \mathbf{j}\cdot\mathbf{E} + r,\\
&\partial_t \mathbf{B} + \operatorname{curl}\mathbf{E} = \mathbf{0},\\
&\operatorname{curl}\mathbf{B} = \mu_0\mathbf{j},
\end{aligned} \tag{2.1}$$

where $\mathbf{j}$ is the electric current density in the plasma and $\mathbf{E}$ is the electric field. The permeability constant of vacuum is $\mu_0 = 1.26\times10^{-6}\,\mathrm{V\,s\,(A\,m)^{-1}}$. While the last equation (Ampere's law) can be viewed as an equation for the current, we need a closure relation for the electric field. This can be obtained from Ohm's law

$$\mathbf{j} = \sigma(T)\,(\mathbf{E} + \mathbf{v}\times\mathbf{B}), \tag{2.2}$$

which gives

$$\mathbf{E} = \mathbf{B}\times\mathbf{v} + \frac{1}{\sigma(T)}\mathbf{j} = \mathbf{B}\times\mathbf{v} + \frac{1}{\sigma(T)}\operatorname{curl}\mathbf{B} \tag{2.3}$$

to enter the induction equation for B in (2.1). The electric conductivity $\sigma(T)$ depends on temperature and is discussed later. The influence of the electric part on the fluid equations of (2.1) comes from the Lorentz force and Ohmic heating in the momentum equation and energy equation, respectively. The fluid flow influences the equations for the electromagnetic field via the velocity in (2.3).

The fluid equations in (2.1) require additional closure relations for stress tensor Π, heat flux $\mathbf{q}$, and internal energy ε, as well as the radiation r. We assume the simplest thermodynamic laws

$$\Pi = -2\mu(T)\,\overline{\operatorname{grad}\mathbf{v}}, \quad \mathbf{q} = -\lambda(T)\operatorname{grad}T, \tag{2.4}$$

where $\overline{\operatorname{grad}\mathbf{v}}$ represents the traceless and symmetric part of the gradient. The viscosity coefficient $\mu(T)$ and heat conductivity $\lambda(T)$ both depend on temperature. The internal energy follows from the temperature-dependent specific heat $c_v(T)$ by

$$\varepsilon(T) = \int_{T_R}^{T} c_v(\tilde{T})\,d\tilde{T} \tag{2.5}$$

with a reference temperature T_R. The radiation r follows from the equations of radiative transfer. In simplified models, the radiation is modeled by the Stefan–Boltzmann law and depends only on temperature $r(T)$.

In MHD, the Lorentz force has typically been transformed into the divergence of the Maxwell tensor and Ohmic heating is eliminated by considering the total energy balance. After this reformulation, the equations for density, velocity and magnetic field read

$$\begin{aligned}
&\partial_t \rho + \operatorname{div}\rho\mathbf{v} = \mathbf{0},\\
&\partial_t \rho\mathbf{v} + \operatorname{div}\left(\rho\mathbf{v}\mathbf{v} + \left(p + \frac{1}{2\mu_0}\mathbf{B}^2\right)\mathbf{I} - \frac{1}{\mu_0}\mathbf{B}\,\mathbf{B}^T\right)\\
&\quad = \operatorname{div}(2\mu(T)\,\overline{\operatorname{grad}\mathbf{v}}),\\
&\partial_t \mathbf{B} + \operatorname{div}\left(\mathbf{B}\,\mathbf{v}^T - \mathbf{v}\,\mathbf{B}^T\right) = -\operatorname{curl}\left(\frac{1}{\sigma(T)}\operatorname{curl}\mathbf{B}\right),
\end{aligned} \tag{2.6}$$

and for the total energy

$$E_{tot} = \rho\left(\varepsilon(T) + \frac{1}{2}\mathbf{v}^2\right) + \frac{1}{2\mu_0}\mathbf{B}^2, \tag{2.7}$$

including internal, kinetic and magnetic energy, we have the total energy balance

$$\partial_t E_{tot} + \operatorname{div}\left(\left(E_{tot} + p + \frac{1}{2\mu_0}\mathbf{B}^2\right)\mathbf{v} - \frac{1}{\mu_0}\mathbf{B}(\mathbf{B}\cdot\mathbf{v})\right)$$
$$= \operatorname{div}\left(\frac{1}{\mu_0\sigma(T)}\mathbf{B}\times\operatorname{curl}\mathbf{B} + 2\mu(T)\mathbf{v}\cdot\overline{\operatorname{grad}\mathbf{v}}\right.$$
$$\left.+\lambda(T)\operatorname{grad}T\right) + r(T), \tag{2.8}$$

which serves as an equation for temperature.

The equations above represent a strongly coupled system to describe the plasma flow in an electric arc. Usually, the mechanical equations and the heat transfer are split from the electrodynamic part in a weak coupling approach, for example in Zheng et al. (2004). In the following, we investigate a different coupling in the magnetic diffusion, and heat transfer is strongly coupled.

2.2. Non-convective case

When neglecting the flow of the plasma $\mathbf{v} \equiv \mathbf{0}$, the remaining relevant equations are

$$\partial_t\mathbf{B} = -\operatorname{curl}\left(\frac{1}{\mu_0\sigma(T)}\operatorname{curl}\mathbf{B}\right), \tag{2.9}$$

$$\partial_t\left(\rho\varepsilon + \frac{1}{2\mu_0}\mathbf{B}^2\right) = \operatorname{div}\left(\frac{1}{\sigma(T)}\mathbf{B}\times\operatorname{curl}\mathbf{B}\right.$$
$$\left.+\lambda(T)\operatorname{grad}T\right) + r(T), \tag{2.10}$$

for the magnetic field and temperature. These equations model the dissipation of the plasma, while the remainder of (2.6) and (2.8) represent the convection of an ideal non-dissipative plasma. The second equation can be reduced to a diffusion equation for temperature when eliminating the magnetic energy. We find the non-convective model for plasma

$$\partial_t\mathbf{B} = -\operatorname{curl}\left(\frac{1}{\sigma(T)}\operatorname{curl}\mathbf{B}\right),$$
$$\rho c_v(T)\partial_t T = \operatorname{div}(\lambda(T)\operatorname{grad}T) + \frac{1}{\sigma(T)\mu_0}(\operatorname{curl}\mathbf{B})^2 + r(T) \tag{2.11}$$

consisting of two nonlinear diffusion-reaction equations. These equations describe the interplay of nonlinear magnetic and temperature diffusion coupled by the electrical conductivity $\sigma(T)$ and linked to Ohmic heating and radiation.

2.3. Model discussion

2.3.1. Electric conductivity. The essence of the model described here lies in the choice of the temperature-dependent electric conductivity $\sigma(T)$. This function models the neutral gas, the ionization and full plasma behavior over the whole temperature range. While the conductivity is well defined for temperatures which produce a sufficient degree of ionization, it is less simple for low temperature where the medium is essentially neutral.

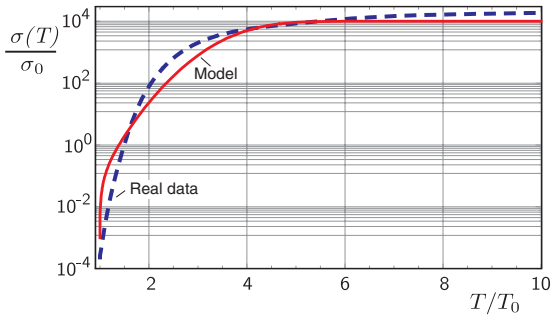

Figure 1. (Colour online) Comparison of electric conductivity given by the model (2.12)/(2.13) and realistic data from Huguenot (2008) with $\sigma_0 = 10^4\,\mathrm{A\,(V\,m)^{-1}}$ and $T_0 = 3000\,\mathrm{K}$.

When modeling electric arcs, the conductivity typically depends not only on temperature but also on the electric field present in the gas (see Raizer 1991). An electric field induces some ionization even at low temperature and produces a non-vanishing electric conductivity.

In this paper, we simplify the situation and assume a pure temperature dependence for σ, which is very small but non-vanishing for low temperature. We think of a background electric field that justifies this assumption. As a model for conductivity, we will employ the erf-type function

$$s(T,\sigma_{\min},\sigma_{\max},\bar{T},\varepsilon) = \sigma_{\min} + \frac{\sigma_{\max}-\sigma_{\min}}{1-\operatorname{erf}(\frac{T_0-\bar{T}}{\varepsilon T_0})}$$
$$\times\left(\operatorname{erf}(\frac{T-\bar{T}}{\varepsilon T_0}) - \operatorname{erf}\left(\frac{T_0-\bar{T}}{\varepsilon T_0}\right)\right), \tag{2.12}$$

which is controlled by a minimum $\sigma_{\min}$ at temperature T_0, a maximum conductivity $\sigma_{\max}$ for large temperatures, a transition temperature $\bar{T}$, and a transition slope ε^{-1}. Figure 1 compares the model with

$$\sigma_{\min} = 10^{-7}\sigma_0, \quad \sigma_{\max} = \sigma_0, \quad \bar{T} = 4T_0, \quad \varepsilon = 1 \tag{2.13}$$

to realistic measurements for sulfur hexafluoride (SF_6) gas obtained from Huguenot (2008). The electric conductivity spans at least seven orders of magnitude and the qualitative behavior is reasonably captured by the model. Below, we will use different values for $\sigma_{\min}/\sigma_{\max}$ as well as further reduced models for $\sigma(T)$ to obtain qualitative insight into the behavior of electric arcs.

2.3.2. Energy dissipation. In both full MHD and the non-convective model (2.11), energy is dissipated through heat conduction and radiation. In high-pressure arcs, radiation is a major contribution to energy loss. It typically occurs in two variants, the local energy loss by a Stefan–Boltzmann law (optically thin medium), or an additional contribution to heat conduction (optically thick medium). In order to reduce complexity and allow a transparent qualitative insight, we will neglect local energy loss in this paper. To compensate the energy dissipation, we will assume a larger heat conductivity instead. In this way, we consider only a single energy

dissipation mechanism. Furthermore, the heat conductivity λ is assumed to be independent of temperature, that is $\lambda = \text{const}$. In comparison with the strong dependence of electric conductivity, the variations of λ are negligible (see Huguenot 2008). The inclusion of local losses and nonlinearity of λ is left for future work.

2.3.3. Specific heat/density. For simplicity, we will additionally assume $c_v = \text{const}$ and $\rho = \text{const}$ in the non-convective model (2.11).

2.3.4. Scaling. All quantities including space and time are scaled according to ψ/ψ_0 with some choice of scaling factor ψ_0. The choice of the electric conductivity scale is additionally influenced by the choice of the model as in (2.12). To reduce complexity, we assume

$$\frac{t_0}{\mu_0\sigma_0 x_0^2} = 1, \quad \frac{\mu_0\sigma_0\lambda}{\rho_0 c_v} = 1, \quad \frac{B_0^2}{\mu_0\rho_0 c_v T_0} = 1, \quad \frac{\mu_0 j_0 x_0}{B_0} = 1, \tag{2.14}$$

such that space and time scale follow the magnetic diffusion, magnetic and thermal diffusion scale identically, and the magnetic field occurs on the scale of thermal energy. The current density scale is linked to the scale of the magnetic field by Ampere's law. Some example values satisfying this scaling are given by

$$\begin{cases} \sigma_0 = 10^4 \dfrac{\text{A}}{\text{Vm}}, \quad \lambda = 8\times 10^2 \dfrac{\text{W}}{\text{mK}}, \quad \rho_0 = 10^{-2}\dfrac{\text{kg}}{\text{m}^3}, \\ c_v = 10^3 \dfrac{\text{J}}{\text{kgK}}, \quad T_0 = 3\times 10^3\,\text{K}, \quad B_0 = 0.2\,\text{T}, \\ j_0 = 3\times 10^6 \dfrac{\text{A}}{\text{m}^2}, \quad x_0 = 5\times 10^{-2}\,\text{m}, \quad t_0 = 2.6\times 10^{-5}\,\text{s}, \end{cases} \tag{2.15}$$

which are realistic values for strong electric arcs in SF_6 corresponding to Fig. 1 and (2.12)/(2.13). Only the heat conductivity is one to two orders of magnitude too large in order to compensate for the neglected radiation.

With (2.14), no characteristic dimensionless parameters appear in (2.11). The behavior of the system is influenced by the choice of the conductivity model $\sigma(T)$ and the inhomogeneous boundary conditions.

2.3.5. Numerical issues. After investigating the non-convective model in this paper, we will solve the full MHD equation in a future paper. The MHD system consists of a flow part and dissipation, where the flow is governed by the divergence expressions on the left-hand side in (2.6)/(2.8) and the dissipation by the right-hand side. Furthermore, the dissipation part is nothing but the non-convective model in (2.11).

Based on the findings of this paper, we assume that the essential behavior of the arc is controlled by the dissipation, while the flow is mostly a reaction. Hence, special care and understanding of the dissipation will be worthwhile when designing the numerical method for the full equations in a subsequent paper.

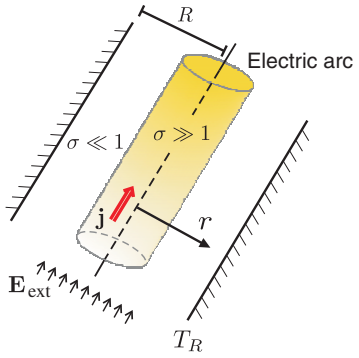

Figure 2. (Colour online) Settings for an infinite axisymmetric arc column in a cylinder. The arc can be driven by an external field or a prescribed total current.

3. Infinite arc column model

To study the properties of the non-convective model (2.11), we first consider an infinite arc column of plasma within a walled cylinder of radius R. The setting is displayed in Fig. 2. We assume axisymmetry and as such all field variables depend only on time and the radius, $r \in [0, R]$. The electric current density points solely along in the direction of the z-axis of the cylinder $\mathbf{j} = (0, 0, j^{(z)})^T$. Hence, the only non-vanishing magnetic field component is in the angular direction $B^{(\varphi)}$. The arc can be driven either by a prescribed total current I_{ext} or an external electric field E_{ext}.

In the following, we want to study the basic mathematical behavior of arc creation and extinction as described by the non-convective model above. As already discussed, the assumptions for the electric conductivity limit the physicality of the model. Still, the model is rich enough to provide interesting mathematical and physical insight.

In axisymmetry, with spatial dependence only on r, (2.11) read

$$\partial_t B^{(\varphi)} = \partial_r\left(\frac{1}{\mu_0\sigma(T)}\frac{1}{r}\partial_r(r\,B^{(\varphi)})\right), \tag{3.1a}$$

$$\partial_t T = \frac{\lambda}{\rho c_v}\frac{1}{r}\partial_r(r\,\partial_r T) + \frac{1}{\rho c_v \sigma(T)}(j^{(z)})^2, \tag{3.1b}$$

for the angular magnetic field $B^{(\varphi)}(r,t)$ and temperature $T(r,t)$. The current density $j^{(z)}(r,t)$ is given by

$$j^{(z)} = \frac{1}{\mu_0 r}\partial_r\left(r\,B^{(\varphi)}\right) \tag{3.1c}$$

and enters the equation for temperature as quadratic Ohmic heating. The equations are homogeneous; hence, any driving force must come from boundary conditions or initial conditions.

At the z-axis, $r = 0$, we assume even and odd symmetry for temperature and angular magnetic field, that

is

$$r = 0: \quad \partial_r T(0,t) = 0, \quad B^{(\varphi)}(0,t) = 0, \tag{3.2}$$

and we fix the temperature at the cylinder wall

$$r = R: \quad T(R,0) = T_0 \tag{3.3}$$

with some given temperature T_0 also used as temperature scale.

In the current-driven process, the total current has to satisfy

$$I_{\text{ext}} = 2\pi \int_0^R j^{(z)}(r) r\, dr = \frac{2\pi}{\mu_0} \int_0^R \partial_r (r\, B^{(\varphi)})\, dr$$
$$= \frac{2\pi R}{\mu_0} B^{(\varphi)}(R) \tag{3.4}$$

from Ampere's law. This gives a Dirichlet boundary condition

$$r = R: \quad B^{(\varphi)}(R,0) = \mu_0 \frac{I_{\text{ext}}}{2\pi R}, \tag{3.5}$$

for the magnetic field. When modeling arc creation we start with homogeneous initial conditions

$$t = 0: \quad T(r,0) = T_0, \quad B^{(\varphi)}(r,0) = 0; \tag{3.6}$$

hence, the external current in the boundary conditions represents the driving force of the process. This setting turns out to be numerically difficult. It also does not correspond to the physical process. Starting with homogeneous initial conditions, an arc is created by applying an external potential difference, by means of an electric field.

In the potential-driven case, we assume an electric potential satisfying $\Delta\varphi^{(\text{ext})} = 0$ within the cylinder with a potential difference at infinity such that the electric field is given by $E_{\text{ext}} = \partial_z \varphi^{(\text{ext})}$. Symmetry and geometry imply that E_{ext} is constant both along the axis of the cylinder and in radial direction. It may, however, depend on time. The electric field enters the Neumann boundary condition for the magnetic field, which reads

$$r = R: \quad \partial_r (r\, B^{(\varphi)})\big|_{r=R} = R\, \mu_0 \sigma(T_0) E_{\text{ext}}. \tag{3.7}$$

In the case of homogeneous initial conditions, the driving force of the process is represented by the electric field.

The Neumann boundary conditions require $\sigma(T_0) \neq 0$, otherwise the system becomes homogeneous and the initial conditions would remain unchanged. If the equations based on the vector potential for the magnetic field were used, the external electric field would enter the equation as a source term and $\sigma(T_0) = 0$ could be imposed. Additionally, it can be shown for the steady case that the solution of (3.1) with (3.7) converges to the vector potential solution for $\sigma(T_0) \to 0$. Hence, it will be part of our model to assume a small but finite electric conductivity at the wall. The reason for sticking to the description based on the magnetic field stems from the usage of the MHD equations (2.6)/(2.8) in the full convective case.

4. Steady arc column solutions

After creating an arc with given electric field, a steady temperature field across the channel will emerge that balances the Ohmic heating due to the current with heat diffusion. The temperature solution in the steady situation satisfies the nonlinear reaction–diffusion equation

$$\frac{1}{r} \partial_r (r\, \lambda\, \partial_r T) = -\sigma(T(r))\, E_{\text{ext}}^2 \tag{4.1}$$

and the fields of current density and magnetic field can be computed by

$$j^{(z)}(r) = \sigma(T(r))\, E_{\text{ext}}, \quad B^{(\varphi)}(r) = E_{\text{ext}} \frac{\mu_0}{r} \int_0^r \sigma(T(\tilde{r}))\tilde{r}\, d\tilde{r} \tag{4.2}$$

from the temperature. Boundary conditions for temperature are given by

$$T(R) = T_0, \quad \partial_r T|_{r=0} = 0 \tag{4.3}$$

in accordance with the description above. In the following, we will investigate (4.1) for different electric conductivity functions $\sigma(T)$ and electric fields E_{ext}. The relevant dimensionless parameter is

$$E := \sqrt{\frac{E_{\text{ext}}^2 R^2 \sigma_0}{\lambda\, T_0}}, \tag{4.4}$$

which describes the ratio between Ohmic heating and heat conduction.

4.1. Linear conductivity

The simplest model for electric conductivity is assuming a linear dependence of the form

$$\sigma(T) = \sigma_0 + \alpha(T - T_0), \tag{4.5}$$

with $\sigma(T_0) = \sigma_0 > 0$ and a slope $\alpha > 0$. The reaction–diffusion equation for temperature (4.1) reduces to a Bessel differential equation with exact solution

$$T(r) = T_0 \left(1 + \frac{E^2}{A} \left(\frac{J_0(\sqrt{A}\, r/R)}{J_0(\sqrt{A})} - 1 \right)\right), \tag{4.6}$$

where J_0 is the zeroth Bessel function of the first kind. The conductivity slope α enters the solution together with the electric field E_{ext}, the heat conductivity λ and the radius of the cylinder R in the dimensionless parameter

$$A = \frac{\alpha E_{\text{ext}}^2 R^2}{\lambda}. \tag{4.7}$$

If the slope α goes to zero, the solution reduces to the parabola

$$T(r) = T_0 \left(1 + E^2 \frac{1}{4} \left(1 - \left(\frac{r}{R}\right)^2\right)\right), \tag{4.8}$$

with maximal temperature $T_{\max} = T_0(1 + E^2/4)$ in the center. For $\alpha > 0$, that is $A > 0$, this maximal temperature increases and becomes infinite when $\sqrt{A}$ reaches the first zero of the Bessel function J_0. For larger values $A > 5.78...$, a positive temperature field

does not exist any longer, due to oscillations of the Bessel function.

If we choose σ_0 very small, this mathematical blowup behavior represents the ignition of an arc. For small slopes, the solution can be interpreted as a temperature field induced by creepage current in a capacitor represented by the infinite cylinder in our case. If the conductivity increase relative to heat conduction, electric field and domain size becomes too large, the nonlinear increase in Ohmic heating cannot be compensated by heat conduction and the temperature tends to infinity. Note that this blowup is independent of the value of $\sigma_0 > 0$. The blowup occurs faster with higher conductivity slope, electric field, larger domain size, and smaller heat conductivity.

4.2. Exponential conductivity

The linear model for electrical conductivity is extremely simplified. If we consider the exponential function

$$\sigma(T) = \sigma_0 \exp\left(\frac{\alpha}{\sigma_0}(T - T_0)\right), \tag{4.9}$$

we expect a more physical result. Here, the parameter α again takes the role of a slope or increase factor of the exponential $\sigma'(T_0) = \alpha$. For $\alpha \to 0$, we have $\sigma(T) = \sigma_0$. The equation for temperature (4.1) can again be solved analytically and gives two different solutions

$$T_{1,2}(r) = T_0 \times \left(1 + \frac{E^2}{A} \ln\left(\frac{8\left(4 - A \mp 2\sqrt{4-2A}\right)}{\left(A + \left(4 - A \mp 2\sqrt{4-2A}\right)\left(\frac{r}{R}\right)^2\right)^2}\right)\right), \tag{4.10}$$

labeled $T_{1,2}$ depending on whether the minus or plus sign is used in the logarithm. As described above, the solution is essentially influenced by the parameter A as given in (4.7). For the slope $\alpha \to 0$ ($A \to 0$), the solution T_1 converges to the parabola for constant conductivity while T_2 becomes infinite. For increasing slopes T_1 grows and T_2 shrinks and both solutions meet for $A = 2$. In case of values $A > 2$, the temperature solution ceases to exist due to complex values in the logarithm.

If we consider the small branch T_1, the interpretation is analogous to the linear model. For small slopes, the temperature corresponds to a creepage current, and beyond a slope or beyond a certain electric field given by $A = 2$ the heat conduction cannot balance the nonlinear Ohmic heating. Note that in this case, the temperature does not blow up. The maximal temperature reached by creepage in this model is $T_1(0)|_{A=2} = T_0(1+\ln(16)\,E^2/4)$.

The second branch T_2 is more difficult to understand at this point.

For a given electric field, the exponential model yields two steady solutions that correspond to a low temperature capacitor solution and an arcing solution exhibiting higher temperature and higher electric conductivity and current. Which of these steady solutions is realized depends on the process.

4.3. Step-shaped conductivity

Both the linear and exponential models for electric conductivity predict a non-existence of solutions for strongly increasing conductivity functions. This nonexistence is unphysical and due to the assumptions that the conductivity may tend to infinity. If we use the function $\sigma(T) = s(T, \sigma_{\min}, \sigma_{\max}, \bar{T}, \varepsilon)$ from (2.12), we have a step-shaped function that starts at $\sigma_{\min}$ at T_0 and increases with temperature rapidly over five orders of magnitude before leveling off to a large constant conductivity $\sigma_{\max}$. We use

$$\sigma_{\min} = 10^{-3}\sigma_0, \quad \sigma_{\max} = 10^2\sigma_0, \quad \bar{T} = 4T_0, \quad \text{and } \varepsilon = 1 \tag{4.11}$$

for the arc column model. This model assumes a somewhat smaller range of values for electric conductivity than real data show, but allows qualitative insight into arcing behavior.

An analytical solution cannot be found. We study this model for various cases of the dimensionless parameter E from (4.4) by solving (4.1) with a shooting method. That is, we prescribe a zero gradient and an estimated value $T^\star$ for the temperature at $r = 0$ and integrate the ordinary differential equation (4.1) as initial value problem up to $r = R$. The estimated value $T^\star$ has to be chosen such that $T(R) = T_0$.

For $E = 1$, we find three different solutions as shown in Fig. 3. One solution shows very little temperature increase and conductivity as well as current stays very low. As before, this solution (*capacitor* solution) is interpreted as creepage current in a capacitor. In another solution, the channel is almost completely filled with highly conducting plasma and correspondingly large temperature (labeled in the remainder as *burning* solution). The intermediate solution shows a conductive region only in the center of the channel and medium temperatures (the *arcing* solution).

When increasing the electric field, that is the parameter E, the capacitor solution changes very little, while the temperature of the burning solution increases and of the arcing solution decreases. For a critical $E_{\text{crit}} = 17.4$, the arcing and capacitor solutions meet and beyond that critical value only the burning solution continues to exist. This behavior is also described by the exponential conductivity above, and the existence of the burning solution is the result of a finite maximal conductivity in the present case.

When decreasing the parameter E, the burning solution shrinks and the arcing solution increases until both solutions meet and vanish such that for very low values of E only the capacitor solution exists.

4.4. Current–voltage characteristics

The behavior of the arc column becomes more clear when considering the diagram of the current–voltage

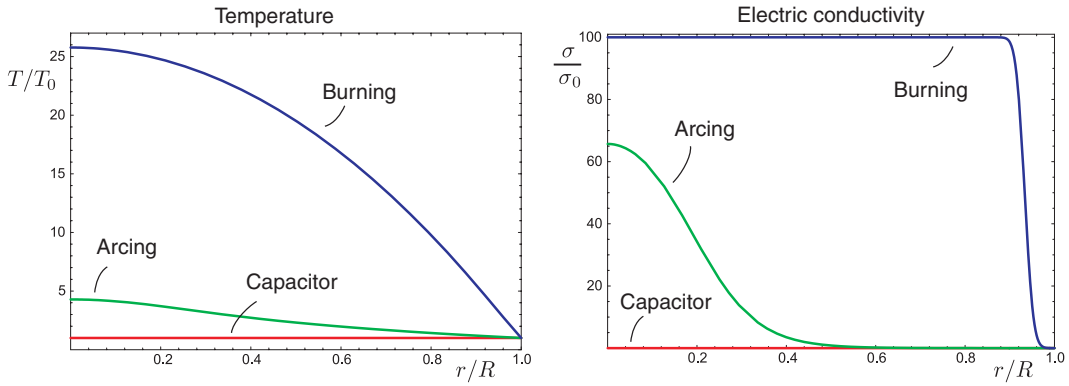

Figure 3. (Colour online) Three possible stationary solutions of the non-convective arc model, labeled by 'capacitor' solution, 'arcing' solution and 'burning' solution.

characteristic. For all solutions found for a given electric field E_{ext}, we can easily calculate the total current flowing through the arc column by

$$I_{\text{tot}} = 2\pi \int_0^R j^{(z)}(r) r \, dr = 2\pi \, E_{\text{ext}} \int_0^R \sigma(T(r;\, E_{\text{ext}}))\, r \, dr, \tag{4.12}$$

where we indicated that the solution T depends on E_{ext} or, to be precise, on the parameter E. The characteristic $E_{\text{ext}} = \psi(I_{\text{tot}})$ gives a relation between the current and the electric field or equivalently the voltage for a given length of the column. We write the characteristic in dimensionless parameters as

$$\sqrt{\frac{E_{\text{ext}}^2 R^2 \sigma_0}{\lambda\, T_0}} = \psi\left(\frac{I_{\text{tot}}}{R\sqrt{\sigma_0 \lambda\, T_0}}\right). \tag{4.13}$$

The function ψ, as obtained for the infinite arc column (4.1) with (4.11), is shown in Fig. 4 and exhibits a non-monotone behavior that is typical for measurements of electric arcs. For an intermediate value of the electric field, the characteristic shows three different values for the total current, which correspond to the capacitor, arcing, and burning solutions. In general, the strongly increasing branch of the characteristic for very low currents represents the capacitor solution. The arcing solution is found along the decreasing branch until a minimum electric field. Finally, the slowly increasing branch gives the burning solution. The slope of the capacitor and burning branch is almost constant, indicating an Ohm relation with a resistivity coefficient determined from the minimal and maximal electric conductivity in the model. The critical value $E_{\text{crit}} = 17.4$ mentioned above can also be read off the figure.

The question remains what solution will be established in a time-dependent simulation. We will see that the decreasing branch represents unstable processes.

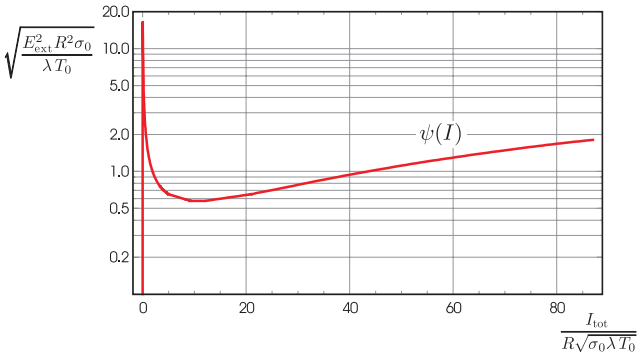

Figure 4. (Colour online) Current–voltage characteristics for a steady infinite arc column in a cylinder parameterized with dimensionless electric field and total current. The typical non-monotone behavior is visible.

5. Unsteady arc column

We now consider the time-dependent equations (3.1) for the infinite arc column model

$$\partial_t B^{(\varphi)} = \partial_r \left(\frac{1}{\mu_0 \sigma(T)} \frac{1}{r} \partial_r \left(r\, B^{(\varphi)} \right) \right),$$

$$\partial_t T = \frac{\lambda}{\rho c_v} \frac{1}{r} \partial_r \left(r\, \partial_r T \right) + \frac{1}{\rho c_v \sigma(T)} (j^{(z)})^2,$$

where the current density is given by

$$j^{(z)} = \frac{1}{\mu_0\, r} \partial_r \left(r\, B^{(\varphi)} \right)$$

on a domain $r \in [0, R]$ using the step-shaped electrical conductivity (2.12) with parameter values (4.11). Initially, the magnetic field vanishes and the temperature is given by the boundary value T_0 throughout the domain. No current is flowing. At $t = 0$, we assume an external electric field greater than zero, E_{ext}, which enters the model through the Neumann boundary condition (3.7). After observing several possible solutions in the steady case above, it is interesting to study what solution (capacitor, arcing, burning) will appear in an unsteady process and how they are connected. This will be discussed after introducing the numerical method.

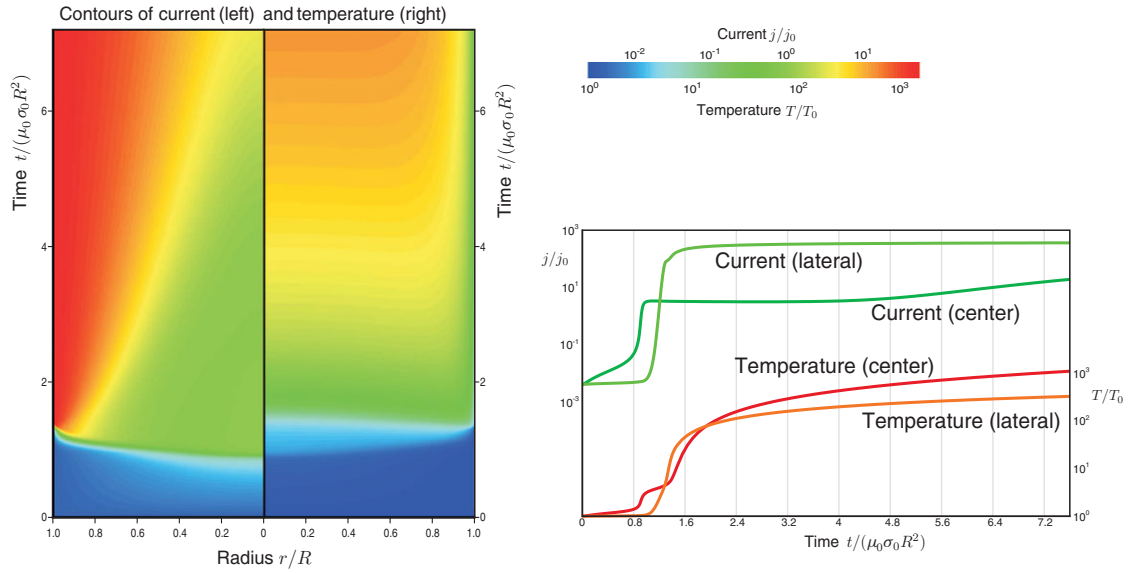

Figure 5. (Colour online) Time evolution of temperature and current in an infinite arc column driven by a fixed external electric field. Right: contours of current and temperature over time and space. Left: time evolution of lateral and center values.

5.1. *Numerical method*

We discretize the domain $r = [0, R]$ using grid size Δr and the spatial derivatives in (3.1) scaled according to (2.14) using second-order finite differences resulting in the semi-discretization

$$\partial_t B^{(\varphi)}\big|_i \approx \frac{1}{\Delta r^2}\left(\frac{1}{\sigma_{i+\frac{1}{2}}}\frac{1}{r_{i+\frac{1}{2}}}\left(r_{i+1}B_{i+1}^{(\varphi)} - r_i B_i^{(\varphi)}\right) - \frac{1}{\sigma_{i-\frac{1}{2}}}\frac{1}{r_{i-\frac{1}{2}}}\left(r_i B_i^{(\varphi)} - r_{i-1}B_{i-1}^{(\varphi)}\right)\right), \tag{5.1a}$$

$$\partial_t T|_i \approx \frac{1}{\Delta r^2}\left(\frac{r_{i+\frac{1}{2}}}{r_i}(T_{i+1} - T_i) - \frac{r_{i-\frac{1}{2}}}{r_i}(T_i - T_{i-1})\right) + \frac{1}{\sigma_i}\left(j_i^{(z)}\right)^2, \tag{5.1b}$$

where

$$j_i^{(z)} \approx \frac{1}{2\Delta r}\left(\frac{r_{i+1}}{r_i}B_{i+1}^{(\varphi)} - \frac{r_{i-1}}{r_i}B_{i-1}^{(\varphi)}\right). \tag{5.1c}$$

For small electrical conductivity, $\sigma(T)$, the equations are very stiff and explicit methods are not competitive. We used TR–BDF2, a second-order L-stable implicit Runge–Kutta scheme, whose first stage is a trapezoidal step and second stage is a second-order backward difference step (see Bank et al. 1985).

5.2. *Arc creation*

The behavior of this process depends on the value of the external field E_{ext}, that is the value of the parameter E in (4.4). For small values, the model will solely establish a small creepage current and come to a steady state according to the capacitor solution. This represents the first steep branch in the characteristic of Fig. 4.

If we start from homogeneous conditions with constant temperature and no current and choose an external field beyond the critical value $E_{\text{crit}} = 17.4$, a capacitor solution becomes inadmissible according to the arc characteristic. The time evolution with $\hat{t} \in [0, 7.5]$ of temperature and current is displayed in Fig. 5 for the case

$$E = 20, \tag{5.2}$$

which is slightly above the critical value. In the figure, temperature is scaled by the boundary value T_0 and current density by the scale

$$j_0 = \frac{B_0}{\mu_0 R} = \frac{1}{R}\sqrt{\frac{\rho_0 c_v T_0}{\mu_0}} \tag{5.3}$$

based on the magnetic field scale. On the left-hand side, the figure shows a contour plot of both current density (left) and temperature (right) in a space–time diagram.

Both levels of current density and temperature are shown in logarithmic scale. Several sharp edges are visible in the contours both of temperature and current indicating transition periods, for example during 'arc ignition' and current diffusion. For a better understanding of the contours, time evolutions of the fields at particular values of r, namely $r = 0.95\,R$ (lateral) and $r = 0$ (center), are plotted on the right-hand side of Fig. 5.

Up to $\hat{t} \approx 0.8$, the system is heated from relatively low conductivity and small currents. The blowup and full formation of the arc happen in two stages between $\hat{t} \approx 0.8$ and $\hat{t} \approx 1.6$. First, the current density in the center grows quickly over several orders of magnitude, heating the temperature in the center to an intermediate value. The high current density together with large temperature values then moves toward the boundary. The high temperature level then leads to a highly conducting plasma, exhibiting a skin effect and concentrating the

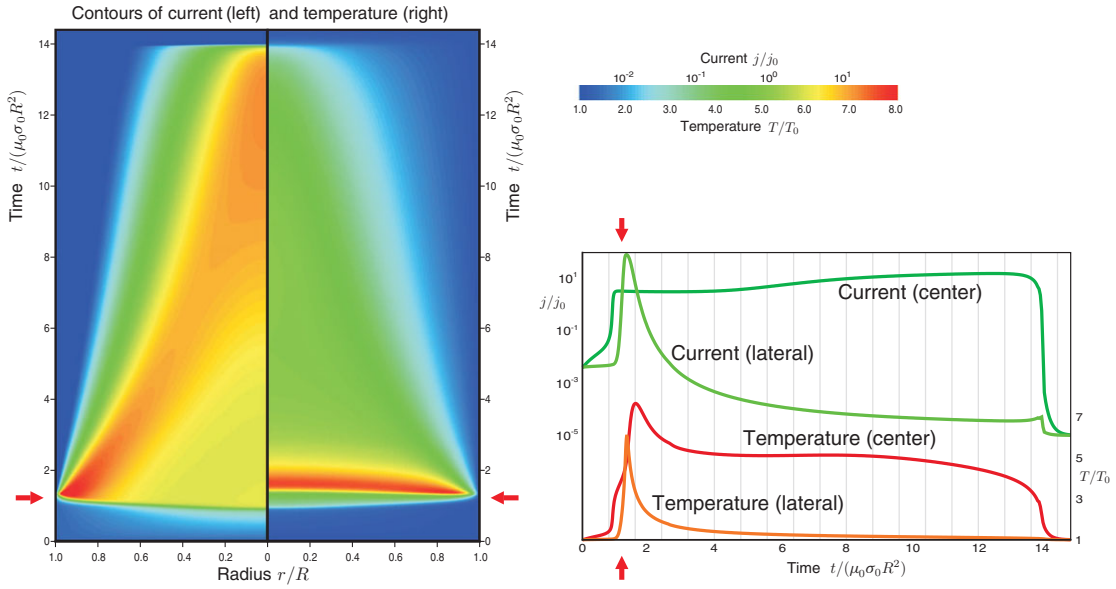

Figure 6. (Colour online) Time evolution of temperature and current in an infinite arc column driven by a fixed external electric field, which is switched down to a small value at $\hat{t} = 30$. Right: contours of current and temperature over time and space. Left: time evolution of lateral and center values.

current near the boundary. For a short time, this leads to a higher lateral temperature value compared with the center. However, the overall heating presumes and the center temperature takes over again quickly. For $\hat{t} > 1.6$, the current density diffuses slowly toward the center while heating the plasma. The final steady state, which is not yet reached in the figure, corresponds to a burning solution in which essentially the whole channel is filled with highly conducting plasma.

Note that both current density and temperature increase to extremely high values which are unphysical. In reality, the arc is created by applying a voltage, that is an external electric field, but once a significant total current is flowing the generator typically is not able to maintain the voltage and reduces it accordingly.

5.3. *Switch-down*

We now consider the same process as in the previous subsection, but switch down the external electric field shortly after the creation of the arc at $\hat{t} = 1.2$. To avoid numerical instabilities, we reduce the parameter E in the boundary conditions smoothly from $E = 20$ to 0.05 in the time interval $\hat{t} \in [1.2, 1.5]$. The value $E = 0.05$ only admits a capacitor solution according to the characteristic in Fig. 4.

The time evolution of this switching process is shown in Fig. 6. The figure uses the same layout as Fig. 5 with contour plots in the space–time diagram on the left and time evolutions of particular values on the right. Only the current density is shown logarithmically, while temperature uses natural scaling. The beginning of the process is identical to Fig. 5 except that the scaling of the time axis is reduced in the present case. The time of the switching is marked in the figure by arrows on the time axes.

The arc does not vanish immediately after switching down the electric field. The lateral current density decreases dramatically; however, the center value remains the same or is even increasing later. This leads to a focusing of the arc in the center of the channel as also visible in the contour plot. A very weak skin effect is visible inside the plasma column. Similar to the current density, the temperature strongly decreases toward the boundary and concentrated in the center. The arc is burning with considerable strength for a relatively long time period and steady temperature profile. It maintains itself through sufficient energy stored in the temperature profile, even though the only steady solution for the acting electric field would be a capacitor solution.

With time, the temperature decreases very slowly. At a certain time, the temperature drops below a value that is needed to maintain the arc. This depends on the functional relation for the electric conductivity. After passing this point, the current density almost instantly falls to the value given by creepage current corresponding to the very low external electric field. Similarly, the temperature dissipates to a very small value slightly above the boundary condition.

5.4. *Stability*

In the above scenario, the capacitor was the only possible solution, which had to be assumed for long-time stationary state. In this section, we consider the same setting again and create the arc from homogeneous initial values with an electric field $E = 20$, as above, but switch down to the value $E = 0.75$, which admits all three solutions (capacitor, arcing, burning) (see Fig. 4). We will consider three different switching times $t = 1.1$, 1.2, 1.3, which all produce different solutions.

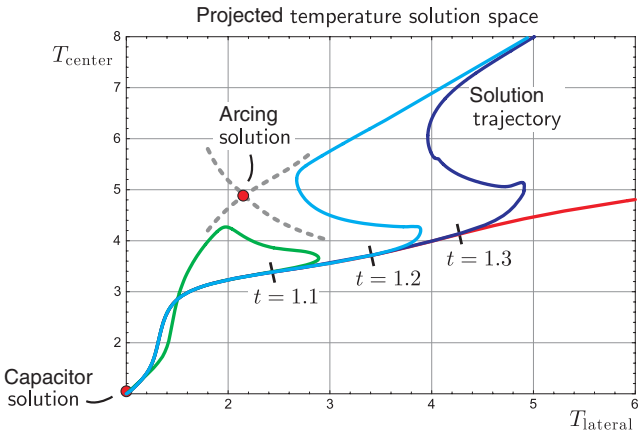

Figure 7. (Colour online) Arc evolutions in the projected temperature solution space. The arc is driven by a strong external field, which is switched down to an intermediate value after some time. Different times result in different solution paths.

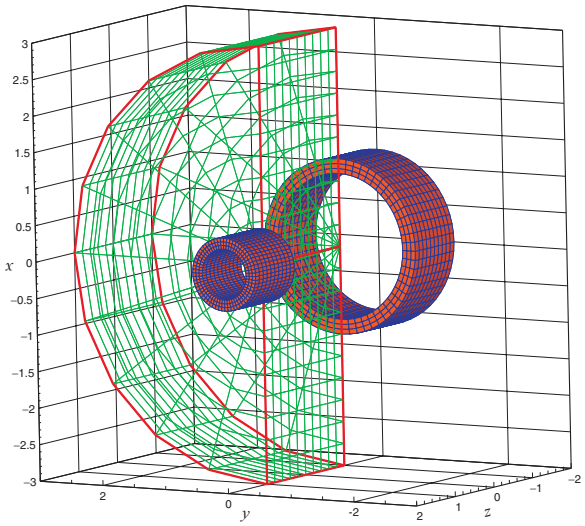

Figure 8. (Colour online) Sketch of geometry for a 3D axisymmetric simulation.

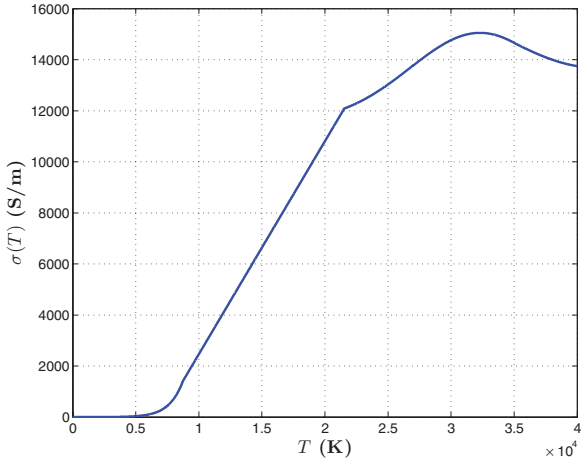

Figure 9. (Colour online) The electrical conductivity $\sigma(T)$ used in the 3D axisymmetric simulations, according to Huguenot (2008).

To allow a better comparison, we display the solution paths of the temperature field. For this, the temperature solution $T(r,t)$ at a certain time t is projected onto the point

$$\tau(t) := (T(r^\star, t), T(0,t)). \tag{5.4}$$

This reduces the infinite dimensional temperature field to a 2D point given by the center value at $r = 0$ and a lateral value at $r^\star = 0.6\,R$. The curve $\tau(t)$ represents the projected solution trajectory and can easily be plotted for different processes. Note that the stationary solutions are represented by points $\tau^{(\text{capacitor})}$, $\tau^{(\text{arcing})}$, and $\tau^{(\text{burning})}$ in the projected temperature solution space.

Figure 7 shows the projected solution space and four different temperature evolutions. All solutions start with homogeneous temperature at the point $\tau(0) = (1,1)$. One trajectory is given by the unswitched process described in Sec. 5.2, shown as red curve (mostly hidden by other curves) leaving the plot in Fig. 7 toward the right. The initial heating phase and ignition is visible when the center temperature increases rapidly. Afterward, both temperatures steadily increase toward the only possible stationary solution (burning) that is situated to the right far outside the plot.

The other three trajectories in Fig. 7 show processes that are started identically to the unswitched case, but switched down at different times. Hence, the solutions follow the red curve initially until the switching time. After switching to the lower electric field $E = 0.75$, the topology of the solution space changes and three stationary points arise representing the capacitor solution near $(1,1)$, the arcing solution in the middle of the plot, and a burning solution that lays outside of the plot beyond the upper right corner. Which solution is finally approached depends on the switch-down time, that is, how much energy has been inserted into the system due to the large electric field. In the case of the two later times $t = 1.2$ and 1.3, the solution approaches the burning solution. On the other hand, when switching down earlier at $t = 1.1$, the final solution will be the capacitor solution, that is the arc extinguishes due to lack of energy. The arcing solution is never assumed as final solution as it turns out to be unstable. This is known in electric engineering from considerations of the current–voltage characteristic (see Maecker 1951; Rieder 1967). Here, it becomes visible from the mathematical behavior of a coupled system of nonlinear reaction–diffusion equations.

Note, however, that the arcing solution is approached from all three trajectories before they bend away. The stationary arcing point is a saddle point in the solution space and consists of an attractive and repulsive submanifold shown as dashed lines in Fig. 7. The neighborhood of the saddle point is relatively flat; hence, the solution trajectories cross this region very slowly. For the lowest trajectory, the situation is similar to the switch-down case discussed above in Sec. 5.3.

After switching down, the arc exists for a fairly long time in which it may be observed as stable. However,

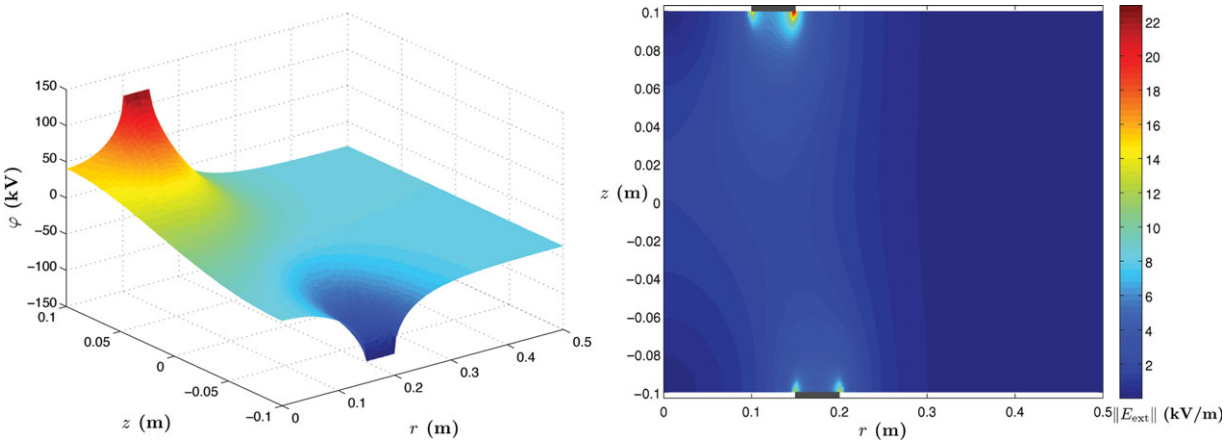

Figure 10. (Colour online) The electric potential φ and applied external electric field $\|\mathbf{E}_{\text{ext}}\|$, the gray rectangles in the right-hand figure depict the position of the contacts.

this is merely a quasi-stability due to the flatness of the neighborhood of the saddle point forcing the solution to change slowly. After sufficient time, all trajectories leave the vicinity of the arcing point either to produce a strong arc or to face extinction. The case decision is made by the amount of energy present in the system.

6. 3D axisymmetric simulations

Using the insights gained by studying the infinite arc column, we now solve the model numerically in 3D axisymmetric cylindrical coordinates mimicking contact geometry typically found in high-voltage circuit breakers and the real material coefficients of SF_6 gas as given in Huguenot (2008).

In 3D axisymmetric cylindrical coordinates, the fields have no angular dependence, that is $B^{(\varphi)} \equiv B^{(\varphi)}(t,r,z)$ and $T \equiv T(t,r,z)$, and the equations for the scaled non-convective model (2.11) become

$$\partial_t B^{(\varphi)} = \partial_r\left(\frac{1}{\sigma(T)}\frac{1}{r}\partial_r\left(rB^{(\varphi)}\right)\right) - \partial_z\left(\frac{1}{\sigma(T)}\partial_z B^{(\varphi)}\right), \tag{6.1a}$$

$$\partial_t T = \kappa\frac{1}{r}\partial_r\left(r\partial_r T\right) + \kappa\partial_z\left(\partial_z T\right) + \frac{1}{\sigma(T)}|\mathbf{j}|^2, \tag{6.1b}$$

where $\mathbf{j} = (-\partial_z B, 0, r\partial_r(rB))^{\mathrm{T}}$. Note that despite the fact we are considering the model in two dimensions, if we assume $B^{(r)} = 0$ and $B^{(z)} = 0$ at $t = 0$, it suffices to only consider the evolution of the φ-component of the magnetic field and the equation for $\mathbf{B}$ becomes scalar.

6.1. Contact modeling and arc initialization

We consider (6.1) in a rectangular domain $(r,z) \in [0,R] \times [-Z,Z]$ and model the initialization of the arc and the position of the contacts as shown in Fig. 8 with an appropriate choice of boundary conditions. Initially, we assume the process is *potential driven* and specify inhomogeneous Neumann boundary conditions for $B^{(\varphi)}$ in terms of the external electric field $\mathbf{E}_{\text{ext}} = (E^{(r)}_{\text{ext}}, 0, E^{(z)}_{\text{ext}})^T$ as

$$\partial_z B^{(\varphi)}|_{z=\pm Z} = \mu_0\sigma(T_0)E^{(r)}_{\text{ext}}, \tag{6.2}$$

$$\partial_r(rB^{(\varphi)})|_{r=R} = R\mu_0\sigma(T_0)E^{(z)}_{\text{ext}}. \tag{6.3}$$

Note that the φ-component of the external electric field is zero since the electric potential has no angular dependence in axisymmetry (see (6.5)). When the total current in the arc, as given by (3.4),

$$I(t,z) = 2\pi\int_0^R r j^{(z)}(r)\,dr = 2\pi\int_0^R r\partial_r B^{(\varphi)}(t,r,z)\,dr = 2\pi R B^{(\varphi)}(t,R,z)$$

is greater than some specified value, that is $I > I_{\max}$, we change the boundary conditions to *current driven*, that is we specify Dirichlet boundary conditions for $B^{(\varphi)}$ on the boundary in terms of the attained current I

$$\begin{aligned} B|_{z=\pm Z} &= \frac{I}{r} && \text{at wall,}\\ \partial_z B|_{z=\pm Z} &= 0 && \text{at contacts,}\\ \partial_r(rB)|_{r=R} &= \frac{I}{R} && \text{at outside wall.}\end{aligned}$$

We denote the time at which the switch from potential to current driven occurs as t_s. The switch from potential to current driven allows us to initialize simulations effectively. This was previously a difficult problem which required an extremely high initial temperature. The arc was then considered to burn in the part of the domain where the gas had not cooled (see Kumar 2009). Although it is a step toward modeling electric arc formation in circuit breakers, it cannot and does not aim to fully capture the true physical process of ignition. The initial conditions used in numerical simulations are given in Sec. 6.3.

The boundary conditions for $B^{(\varphi)}$ together with suitable mixed boundary conditions for the temperature

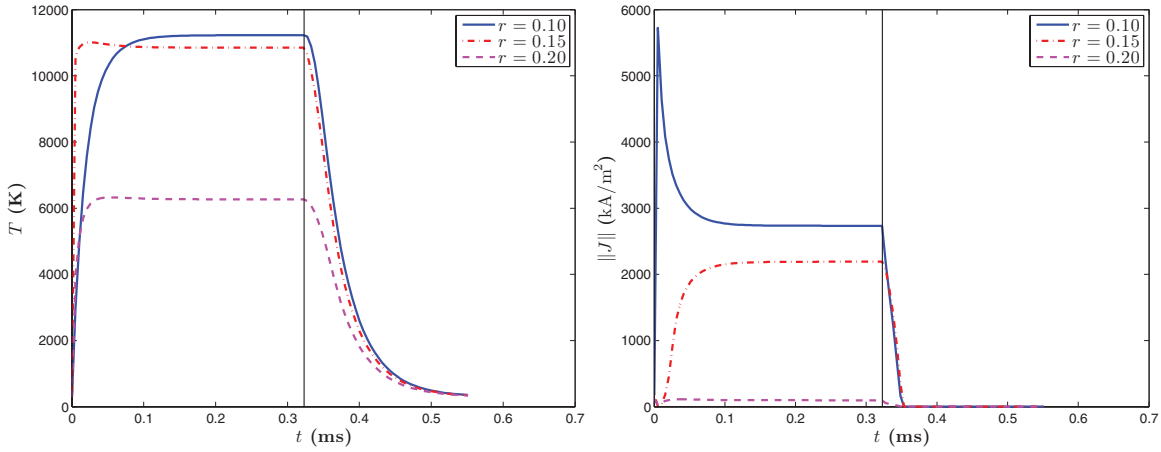

Figure 11. (Colour online) The initial magnetic field B and current density J. The initial temperature is constant $T = 300$ K.

given by

$$T(t,r,z) = T_0 \quad \text{at all none-contact boundaries,}$$

$$\partial_z T|_{z=\pm Z} = 0 \quad \text{at contacts,}$$

model the position of the contacts. Note the boundary conditions for the temperature are independent of the potential- or current-driven mode.

The values of T and $B^{(\varphi)}$ at $r = 0$ in both current- and potential-driven modes are again specified by consider the even, respectively, odd symmetry of the temperature and magnetic fields along the z-axis of the cylinder.

In order to understand why (6.2) models the positions of the contacts appropriately for the potential-driven case, it remains to explain how we specify the components of the electric field $\mathbf{E}_{\text{ext}}$. To calculate the external electric field, we specify the potential across the contacts in terms of $\Delta\phi_0$, solve the Poisson problem

$$\Delta\phi = 0, \tag{6.4a}$$

$$\phi = \pm\Delta\phi_0 \quad \text{at the contacts,} \tag{6.4b}$$

$$\partial\phi = 0 \quad \text{elsewhere,} \tag{6.4c}$$

and calculate the electric field according to

$$\mathbf{E}_{\text{ext}} = -\operatorname{grad}\phi. \tag{6.5}$$

6.2. Discretization

As for the infinite arc column, we use second-order finite differences to discretize the spatial derivatives. The grid is Cartesean with the i-index for the radial and the j-index for the z-coordinate. The semi-discretization of the axisymmetric non-convective model (6.1) becomes

$$\begin{aligned}\partial_t B^{(\varphi)}\big|_{i,j} \approx{}& \frac{1}{\Delta z^2}\left(\frac{1}{\sigma_{i,j+\frac12}}B^{(\varphi)}_{i,j+1} - \frac{2}{\sigma_{i,j}}B^{(\varphi)}_{i,j} + \frac{1}{\sigma_{i,j-\frac12}}B^{(\varphi)}_{i,j-\frac12}\right)\\ &+\frac{1}{\Delta r^2}\left(\frac{1}{\sigma_{i+\frac12,j}}\frac{1}{r_{i+\frac12}}\left(r_{i+1}B^{(\varphi)}_{i+1,j} - r_i B^{(\varphi)}_{i,j}\right)\right.\\ &\left.-\frac{1}{\sigma_{i-\frac12,j}}\frac{1}{r_{i-\frac12}}\left(r_i B^{(\varphi)}_{i,j} - r_{i-1}B^{(\varphi)}_{i-1,j}\right)\right)\end{aligned} \tag{6.6a}$$

for the magnetic field equation and

$$\begin{aligned}\partial_t T|_{i,j} \approx{}& \frac{1}{\Delta z^2}\left(\kappa_{i,j+\frac12}T_{i,j+1} - 2\kappa_{i,j}T_{i,j} + \kappa_{i,j-\frac12}T_{i,j-1}\right)\\ &+\frac{1}{\Delta r^2}\left(\frac{r_{i+\frac12}}{r_i}\kappa_{i+\frac12}\left(T_{i+1,j} - T_{i,j}\right)\right.\\ &\left.-\frac{r_{i-\frac12}}{r_i}\kappa_{i-\frac12}\left(T_{i,j} - T_{i-1,j}\right)\right)\\ &+\frac{1}{\sigma(T_i)}\left(\left(j^{(r)}_{i,j}\right)^2 + \left(j^{(z)}_{i,j}\right)^2\right),\end{aligned} \tag{6.7a}$$

where

$$j^{(r)}_{i,j} \approx -\frac{1}{2dz}\left(B^{(\varphi)}_{i,j+1} - B^{(\varphi)}_{i,j-1}\right), \tag{6.7b}$$

$$j^{(z)}_{i,j} \approx \frac{1}{2\Delta r}\left(\frac{r_{i+1}}{r_i}B^{(\varphi)}_{i+1,j} - \frac{r_{i-1}}{r_i}B^{(\varphi)}_{i-1,j}\right), \tag{6.7c}$$

for the energy balance, where the current components are given by

$$j^{(r)}_{i,j} \approx -\frac{1}{2dz}\left(B^{(\varphi)}_{i,j+1} - B^{(\varphi)}_{i,j-1}\right), \tag{6.8a}$$

$$j^{(z)}_{i,j} \approx \frac{1}{2\Delta r}\left(\frac{r_{i+1}}{r_i}B^{(\varphi)}_{i+1,j} - \frac{r_{i-1}}{r_i}B^{(\varphi)}_{i-1,j}\right). \tag{6.8b}$$

The resulting system of ordinary differential equations is solved by the second-order implicit TR–BDF2 time-integration scheme (Bank et al. 1985).

6.3. Numerical experiment: hollow oblique contacts

We now consider the solution of (6.6)–(6.8a) using $\kappa(T) \equiv$ const and electrical conductivity $\sigma(T) \in [0.2, 1.7\times 10^4]$ fitted to real data as in Fig. 9 (Huguenot 2008; Kumar 2009). The computational domain is $[0, 0.5] \times [-0.1, 0.1]$ m, where the contacts are of width 0.05 m at 0.15–0.20 m at the bottom of the domain and 0.10–0.15 m at the top of the domain; for a schematic of the domain with contacts, see Fig. 10.

We initially specify a temperature of $T_0 = 300$ K and apply an electric potential of 240 kV, that is $\phi_0 = \pm 120$ kV at the contacts. The electric potential and electric field as given by the solution to (6.4) and (6.5) with

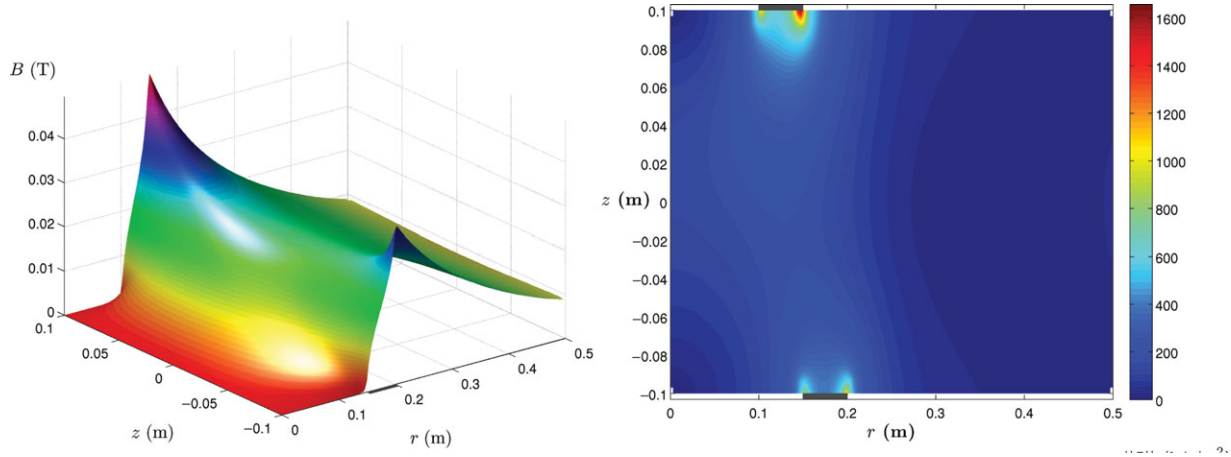

Figure 12. (Colour online) The evolution of $T(t, r, z = 0)$ and $\|J(t, r, z = 0)\|$ at the points $(r, z) = (0.10, 0), (0.15, 0), (0.20, 0)$ inside the circuit breaker. The values of r correspond to the inside of the top contact, the midpoint between the two contacts, and the outside of the bottom contact, respectively. The vertical line at $t = 0.323$ ms represents the time of switch-down. The time of switching from potential to current driven, t_s, occurs at $t = 3.14 \times 10^{-4}$ ms and cannot be seen in this plot.

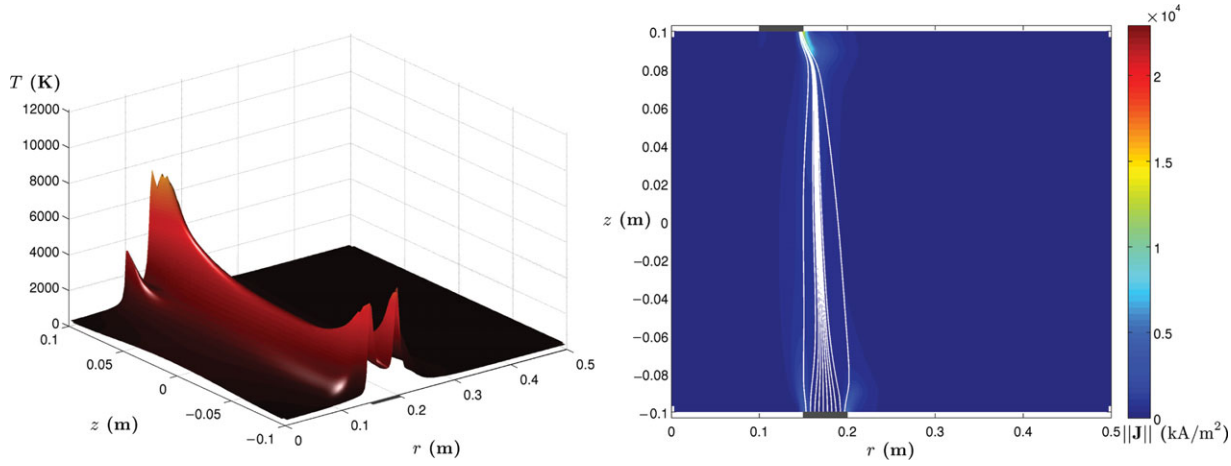

Figure 13. (Colour online) The temperature T and current density J before switching from potential to current driven at $t = 1.57 \times 10^{-4}$ ms ($t = 0.5\, t_s$).

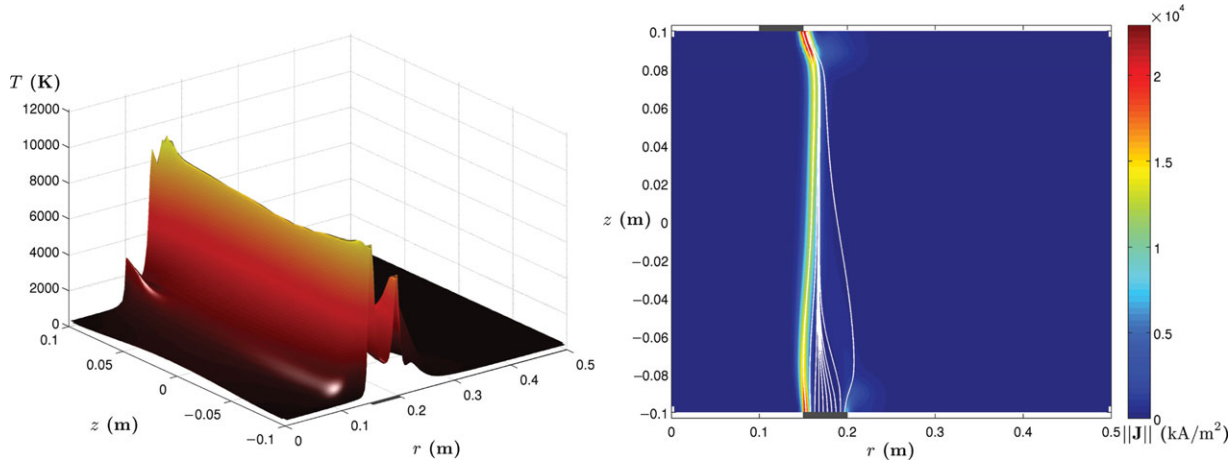

Figure 14. (Colour online) The temperature T and current density J at the point of switching from potential to current driven at $t = 3.14 \times 10^{-4}$ ms.

these values are shown in Fig. 10. The initial condition for $B^{(\varphi)}$ is calculated by solving the stationary problem for (6.6) with the potential-driven boundary conditions (6.2), shown in Fig. 11. Due to the non-constant value of $B^{(\varphi)}$, there is an initial creepage current between the contacts (see Fig. 12). Furthermore, we specify that the simulation switches from potential driven to current driven when the total current in the circuit breaker has

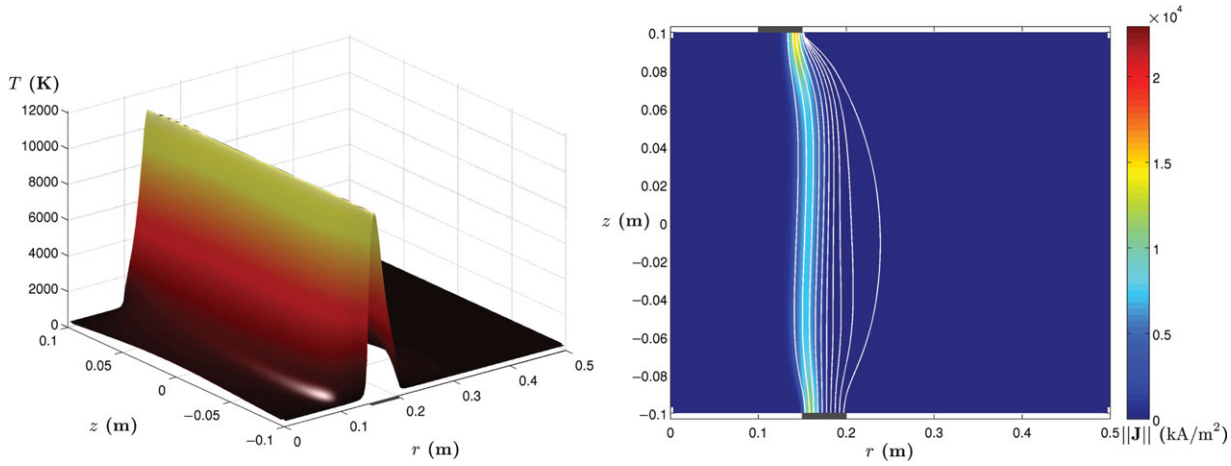

Figure 15. (Colour online) The temperature T and current density J at $t = 3.14 \times 10^{-3}$ ms ($t = 10\,t_s$).

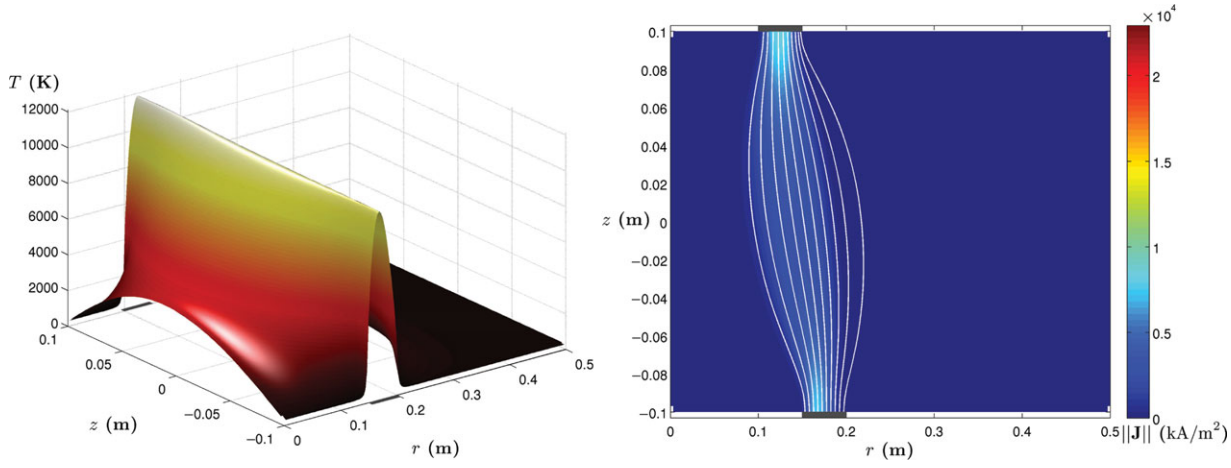

Figure 16. (Colour online) The temperature T and current density J at $t = 3.14 \times 10^{-2}$ ms ($t = 100\,t_s$).

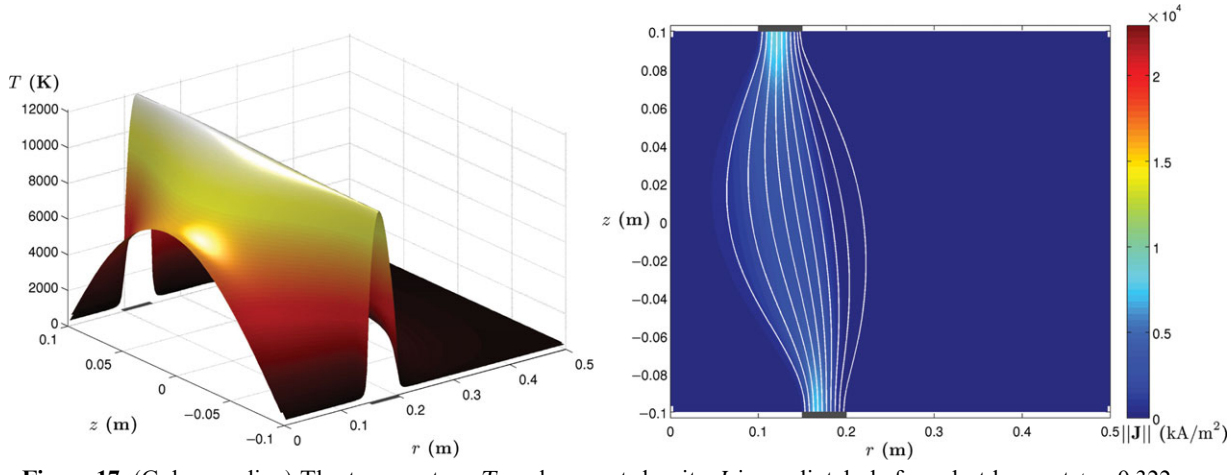

Figure 17. (Colour online) The temperature T and current density J immediately before shutdown at $t = 0.322$ ms.

reached $I_{\max} = 200\,\text{kA}$. In this example, the switch to current driven occurs at $t_s = 3.14 \times 10^{-7}\,\text{s}$ and after the solution has attained a steady state, we *switch down* the electric arc by reverting back to potential-driven boundary conditions, but with negligible $\mathbf{E}_{\text{ext}}$, which occurs at $t = 3.22 \times 10^{-4}\,\text{s}$.

Clearly, the potential-driven phase occurs on a very different scale to the rest of the solution, also depicted in Fig. 12. We see that in Figs. 13 and 14 the current density is initially concentrated around the corners of the contacts before forming a narrow arc of very high current density, which we consider to be modeling the skin effect. We also see that before switching to current driven, very high temperatures are already attained within the arc where current is flowing.

After switching to current driven, the total current in the arc is held constant and the current density within the arc diffuses inward toward the z-axis and is more evenly distributed across the contacts. We see from the temperature that the gas within the device heats up accordingly, leading to higher electrical conductivity. This leads to development of a well-formed electric arc burning between the contacts, as can be seen in Figs. 14–16. Note the largest value attained by the magnetic field is $B = 0.286$ T at $t = 0.322$ ms, immediately before the shutdown of the electric arc (see Fig. 17).

For the shutdown, the simulation is switched to a voltage-driven situation at $t = 0.322$, but with a vanishing external voltage. In contrast to the 1D case, no pseudo-stable arc is observed, instead the arc vanishes quickly after the switch (see Fig. 12). However, the temperature remains high, which results in re-creation of the arc in an alternating current situation.

7. Conclusion

We presented a comprehensive study of the mathematical features of the magnetothermal system that describes electric arcs. The equations, based on the strongly coupled MHD system for plasma flows, consist of Ohmic heating and nonlinear electric conductivity, which are the core components of arcing processes. The non-uniqueness and stability features of the model can be linked to actual physical properties of the electric arc. Even though the model is very rough and does not include important features like radiation or dielectric breakdown, it allows a qualitative description of arc creation and extinction.

The paper also presents 3D axisymmetric simulations of the model, which use strongly coupled numerical methods. In contrast to weakly couple electrodynamics to the heat transfer, the approach of this paper solves heat transfer and magnetic diffusion in a single time integration. Future work will include the coupling of the actual flow and an external electric network. The aim is to contribute to electric arc simulations, for example in the case of very high current circuit breakers.

References

Bank, R. E., Coughran, W. M., Fichtner, W., Grosse, E. H., Rose, D. J. and Smith, R. K. 1985 Transient simulation of silicon devices and circuits. *IEEE Trans. Computer-Aided Des.* **4**, 436–451.

Cassie, A. M. 1939 Arc rupture and circuit severity. A new theory. In: *Conference des Grands Reseaux Electriques*, Electrical Research Association Technical Report, E.R.A. Vol. 108, Springer, 14 pp.

Delmont, P. and Torrilhon, M. 2012a Convective magnetohydrodynamical modeling and simulation of electric arcs. In: Europhysics Conference Abstracts Vol. 36F ISBN 2-914771-79-7. *39th EPS Conference on Plasma Physica & 16th International Congress on Plasma Physics*, 2–6 July 2012, Stockholm, Sweden (ed. S. Ratynsakaya, L. Blomberg, A. Fasoli) p. P1.138.

Delmont, P. and Torrilhon, M. 2012b Magnetohydrodynamical modeling and simulations of electric arc extinction in a network. In: *CD-ROM Proceedings of the 6th European Congress on Computational Methods in Applied Sciences and Engineering (ECCOMAS 2012)* (ed. H. J. Rammerstorfer, F. G. Eberhardsteiner and J. Bhm). Vienna, Austria: Vienna University of Technology.

Finkelnburger, W. and Maecker, H. 1956 Elektrische Bögen und thermische plasmen. In: *Handbuch der Physik* (ed. S. Flügge). Berlin: Springer, pp. 254–440.

Garzon, R. D. 2002 *High Voltage Circuit Breakers: Theory and Design*. New York: CRC Press.

Gleizes, A., Gonzales, J. J. and Freton, P. 2005 Thermal plasma modelling. *J. Phys. D: Appl. Phys.* **38**, 153–183.

Goedbloed, J. P. H. and Poedts, S. 2004 *Principles of Magnetohydrodynamics With Applications to Laboratory and Astrophysical Plasmas, Cambridge University Press*, Cambridge, UK.

Huguenot, P. 2008 Axisymmetric high current arc simulations in generator circuit breakers based on real gas magnetohydrodynamics models. *PhD thesis*, ETH.

Kosse, S., Wendt, M., Uhrlandt, D., Weltmann, K.-D. and Franck, Ch. 2007 Simulation of moving arcs. *Pulsed Power Conference* pp. 1013–1017.

Kumar, H. 2009 Three dimensional high current arc simulations for circuit breakers using real gas resistive magnetohydrodynamics. *PhD thesis*, ETH.

Maecker, H. 1951 Der elektrische lichtbogen. *Ergebnisse der Exacten Naturwissenschaft* **25**, 293–358.

Maximov, S., Venegas, V., Guardado, J. L. and Melgoza, E. 2009 A method for obtaining the electric arc model parameters for SF6 power circuit breakers. IEEE EUROCOM 2009 International Conference Devoted to the 150th Anniversary of Alexander Popov, St. Petersburg, Russia, 13–23 May 2009, pp. 458–463. Red Hook, NY: Curren Associates.

Mayr, O. 1943 On the theory of electric arc and its extinction. *Electrotechnische Zeitschrift ETZ* **64**, 645–652.

Mayr, O. 1955 On the stability limits of switching arcs. *Applied Scientific Research, Section B (Electrophysics, Acoustics, Optics, Mathematical Methods)* **5**, 241–247.

Raizer, Yu. P. 1991 *Gas Discharge Physics*. New York: Springer.

Rieder, RW. 1967 *Plasma und Lichtbogen*. Berlin: Vieweg.

Torrilhon, M. 2007 Uniqueness and stability of a reduced arc model. *Proc. Appl. Math. Mech.* **7**(1), 1141301–1141302.

Tseng, K.-J., Wang, Y.-M. and Vilathgamuwa, D. M. 1997 Experimentally verified hybrid cassie-mayr electric arc model for power electronic simulations. *IEEE Trans. Power. Elect.* **12**(3), 429–437.

Van Der Sluis, L. 2001 *Transients in Power Systems*. New York: John Wiley & Sons.

Zehnder, L., Kiefer, J., Braun, D. and Schönemann, T. 2002 SF6 generator circuit-breaker system for short-circuit currents up to 200 kA. *ABB Technology Review* **3**, 34–40.

Zheng, S., Liu, J.-Y., Gong, Y. and Wang, X.-G. 2004 Two-dimensional numerical simulation on evolution of arc plasma. *Vacuum* **73**, 373–379.